PHYSICAL REVIEW B VOLUME 47, NUMBER 11 15 MARCH 1993-I

# Elementary excitations in cylindrical tubules

M. F. Lin and Kenneth W.-K. Shung
*Physics Department, National Tsing Hua University, Hsinchu, Taiwan 30043, The Republic of China*
(Received 23 October 1992)

A detailed study of the elementary excitations of an electron gas confined to a tubule system is presented. The system could consist either of a single cylindrical tubule or of several tubules sharing a common axis. Graphene tubules with a radius as small as 11 Å have been recently realized. Essential features revealed from this study are expected to be common to the graphene tubules. The dielectric function of the quasi-one-dimensional (1D) tubular system has been evaluated exactly within the random-phase approximation, where both the intrasubband and the intersubband excitations are included. The angular momentum ($L$) is conserved in the tubule system. The excitations, e.g., plasmons, of different $L$'s are thus mutually decoupled. At any given $L$, only a small number of plasmon branches exist, every one of which can be studied systematically. Intertubule interaction for coaxial tubules has been included. The coupling among coaxial tubules adds unique features that distinguish the tubules from other quasi-1D systems.

## I. INTRODUCTION

Recently, Iijima[1] reported observation of the coaxial tubules made of graphitic carbon. A graphene tubule is just a graphitic sheet that is rolled up in the cylindrical form. One of the graphene tubules consists of only two rolled up graphitic sheets, and the smallest graphene tubules have a diameter as small as 22 Å. The small diameter suggests its property to be quasi-one-dimensional (1D). The graphene tubules are closely related to vapor-grown carbon fibers[2] which have considerably larger diameters ($\sim 10$ $\mu$m). Charge carriers could be introduced onto the graphene tubules in a controlled manner by means of intercalation, as could be done for carbon fibers[2] or $C_{60}$ (Ref. 3) molecules. In this work, we have studied the elementary excitations of the interactive charge carriers confined in quasi-1D tubules. Due to the cylindrical symmetry of the system, we were able to derive the exact results within the random-phase approximation (RPA).

A graphene tubule is made of a graphitic sheet. The tubule and the sheet, therefore, are expected to share some common properties. Our previous studies[4] on the graphite intercalation compounds (GIC's) have demonstrated a close similarity between the graphite system and an electron gas, but with a noted difference that the inter-$\pi$-band excitations in graphite are absent in the electron-gas model. We thus approximate the charge carriers on the tubule by a free-electron gas, and hope that such a model could serve as a first step toward a full understanding of the elementary excitations in the graphene tubules. We noted that Dresselhaus, Dresselhaus, and Saito[5] have studied symmetries of carbon atoms in the graphene tubules.

The cylindrical tubules closely resemble other quasi-1D electron systems in, e.g., semiconductor quantum wires (QW's), which have attracted many studies.[6–9] Li and Sarma[6] calculated the excitation spectra of the QW's within the RPA, and found good agreement with experiments.[7] The RPA is also employed here for the calculation. The theory is actually simpler for the tubules since the excitations of different angular momentum ($L$) are decoupled here but not so in a QW. Decoupling of the angular momentum means that the intrasubband excitations ($L=0$) and the intersubband excitations ($L\neq 0$) are independent of each other, and so are the dielectric functions of different $L$'s. This contrasts greatly from the complicated coupling among different excitations in an ordinary QW.[6] The relevant energy scales of the two quasi-1D systems are also very different. While it usually involves meV in semiconductor microstructures, energies in a graphene tubule are of the order 0.1 eV. The small radius of the tubule ($\sim 10$ Å) makes the energy difference between subbands large. On the other hand, its Fermi energy ($E_F$) is expected to be $\sim 0.5-1.0$ eV—if the charge carriers are introduced through intercalation as in GIC's.[2] Large $E_F$ implies that the $T=0$ treatment of this study is a good approximation. Large energy difference between the subbands assures that only few subbands are occupied—a necessary condition for the system to remain quasi-1D. At such an energy scale, the quasi-1D excitations can probably be observed conveniently. There is still another special feature about the graphene tubules: several tubules of different radii may exist coaxially. The coupling among the coaxial tubules adds a unique flavor to this interesting graphite system. The rich physics of the graphene tubules encourages further studies, both theoretical and experimental.

This paper is organized as follows. In Sec. II, the dielectric function of an electron gas confined to a cylindrical tubule is studied within the RPA. The frequency and the oscillator strength of the plasmon modes are evaluated. The results are useful for the subsequent discussions. In Sec. III, an exact formalism of the dielectric function of an $n$-tubule system is developed. Approximated schemes are also developed to analyze the properties of the plasmons. In particular, plasmons of the $n=2$ systems have been evaluated and discussed in details. Concluding remarks are given in Sec. IV.

 

## II. EXCITATIONS IN A CYLINDRICAL TUBULE

A free-electron gas confined to a cylindrical tubule lying on the $z$ axis is considered here. The electrons can move freely in the axial direction. The azimuthal angle ($\phi$) is quantized due to the boundary condition that the wave function is single-valued as $\phi$ is increased by $2\pi$. The electron wave function is therefore

$$|k,l;r_1\rangle = e^{ikz}e^{il\phi}\delta(r-r_1)/\sqrt{r} \ ; \tag{1}$$

where $l=0,\pm1,\pm2,\ldots$ and $r_1$ is the radius of the tubule. The $\delta$ function describes the confinement that electrons stay on the tubule. The state with the momentum $k$ and the angular momentum $l$ has the energy ($\hbar=1$)

$$E(k,l)=k^2/2m^*+l^2/2m^*r_1^2 \ , \tag{2}$$

where $m^*$ is the effective mass, and $l$ serves as the subband index. In ordinary QW's, it is the quantum confinement of electrons to the wire that causes the subband structure; here, it is the periodical boundary condition in $\phi$. We note that, in the latter, subbands with the indices $\pm l$ are degenerate in energy. Only certain subbands are occupied at a given electron density. Here we study the case where the lowest five subbands ($|l|\leq 2$) are occupied. The result could be easily generalized to other cases. The electron density in a graphene tubule could probably be controlled by, e.g., intercalation, as in GIC's.[2] Parameters used for the numerical calculation will be introduced later. With the wave functions expressed by Eq. (1), the Coulomb interaction for electrons on the tubule is

$$V(q,L;r_1)=4\pi e^2 I_L(qr_1)K_L(qr_1) \ . \tag{3}$$

$I_L(qr_1)$ [$K_L(qr_1)$] is the modified Bessel function of the first (second) kind of the order $L$. $L$ and $q$ are recognized to be, respectively, the angular momentum and the momentum transfer of the interaction. The matrix elements of both the intrasubband interaction [$V(q,L=0;r)$, solid and solid-starred curves] and the intersubband interaction [$V(q,L=1;r)$, solid circles and squares] are shown at two tubular radii, $r_1$ and $r_2$ ($r_2>r_1$), in Fig. 1. $V(q,0;r)$, like in a 1D system, is logarithmically divergent as $qr\to 0$, while $V(q,1;r)$ approaches a finite value at small $q$. $V(q,L;r)$ of all $L$ varies as $1/qr$ at large distances ($\sim 1/q \gg r$), which is a characteristic of the 2D Coulomb interaction. Such 1D behavior at distance $\sim 1/q \ll r$ and 2D behavior at $\sim 1/q \gg r_1$ are similar to those found in semiconductor QW's.[8,9] Also shown in Fig. 1 are intertubule interaction, $V(q,L;r_1,r_2)$, which is discussed in Sec. III.

Here in the matrix element of the Coulomb interaction [Eq. (3)] lies the major difference between the tubules and the semiconductor QW's. While the matrix element in the latter has four indices[6] describing the initial and the final states involved in the scattering, Eq. (3) only depends on the angular momentum change, $L$. This angular momentum conservation greatly simplifies the calculation. Most importantly, the dielectric functions, as a result, are diagonalized in $L$. Unlike in a QW where all

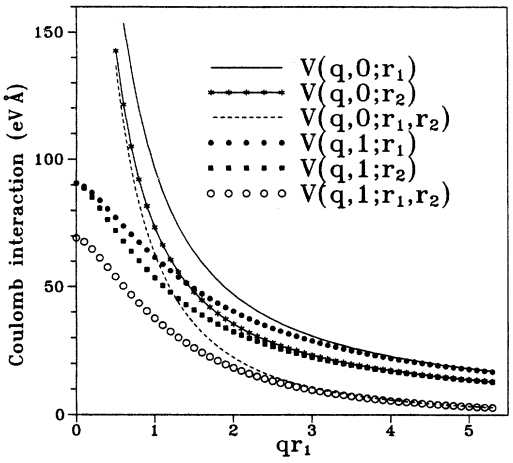


FIG. 1. Plot of the Coulomb interaction vs $qr_1$. Here, $r_1=11$ Å and $r_2=14.4$ Å. Both the intratubule interaction [$V(q,L;r)$] and the intertubule interaction [$V(q,L;r_1,r_2)$] are given. $L=0$ and 1 are, respectively, for the intrasubband and the intersubband interactions.

excitations are coupled together,[8,9] here in the graphene tubules the intrasubband ($L=0$) and the intersubband excitations ($L\neq 0$) are completely decoupled from each other. The interaction matrix element, Eq. (3), would have been different if the actual Bloch states of a graphite layer,[10] instead of $|k,l;r_1\rangle$ of Eq. (1), were used. The angular momentum, however, must still be conserved. So, many of the features discussed here can be readily generalized for graphene tubules.

The dielectric function of a tubule can be determined with the use of the self-consistent-field method,[11] which is equivalent to the RPA. The result is expressed by

$$\epsilon(q,L,w)=\epsilon_0-V(q,L;r_1)\chi(q,L,w) \ , \tag{4}$$

where $\epsilon_0$ is the background dielectric constant. $\chi(q,L,w)$ is the response function (the RPA bubbles):

$$\chi(q,L,w)\equiv\sum_{l}^{\text{occ}}\chi^l(q,L,w) \ , \tag{5a}$$

where

$$\mathrm{Re}\chi^l(q,L,w)=\frac{m^*}{2\pi^2 q}\ln\left|\frac{w^2-E_-^2(q,l,L)}{w^2-E_+^2(q,l,L)}\right| \tag{5b}$$

and

$$\mathrm{Im}\chi^l(q,L,w)=\begin{cases}\dfrac{m^*}{2\pi^2 q} & \text{if } |E_-(q,l,L)|<w<|E_+(q,l,L)| \\ \dfrac{-m^*}{2\pi^2 q} & \text{if } |E_+(q,l,L)|<w<|E_-(q,l,L)| \\ 0 & \text{otherwise} \ .\end{cases} \tag{5c}$$

It should be noticed that every occupied subband has independent [Eq. (5a)], but similar contributions [Eqs. (5b) and (5c)] to $\chi$ of a tubular system. In these expressions

$$E_{\pm}(q,l,L)=\frac{q^2\pm 2k_F(l)q}{2m^*}+\frac{L^2+2lL}{2m^*r_1^2}\ , \tag{6}$$

where $k_F(l)$ is the Fermi momentum of the $l$th subband. $|E_{\pm}(q,l,L)|$ describes the boundary within which the $e$-$h$ excitations are nonvanishing. It is clear from Eqs. (5) and (6) that $\chi$ of different $L$'s are similar in the structure—their only difference stems from their different excitation energies (i.e., different $E_{\pm}$). As a result, $\epsilon(q,L,w)$ of different $L$'s are similar in structure too, and so are their plasmon modes. This fact makes analysis of plasmons particularly simple, since we then only need to study plasmons of certain $L$'s and to draw inferences from the results for other modes. We show in the following that a study on the $L=0$ and $L=1$ plasmons is sufficient for this purpose.

$\epsilon(q,L,w)$ must satisfy the $f$-sum rule which follows from the conservation of the number of particles:[12]

$$\int_0^{\infty} w\ \mathrm{Im}\left\{\frac{-1}{\epsilon(q,L,w)}\right\}dw=\frac{\pi}{2\epsilon_0}w_0^2(q,L)\ , \tag{7}$$

where

$$w_0^2(q,L)=V(q,L;r_1)\left[\frac{L^2}{2m^*r_1^2}+\frac{q^2}{2m^*}\right]\sum_l\frac{2k_F(l)}{\pi^2} \tag{8}$$

is proportional to the total carrier density. One can show that $\epsilon(q,L,w)=\epsilon_0-w_0^2(q,L)/w^2$ as $w\to\infty$. $w_0(q,L)$ is approximately the plasmon frequency at $q\to 0$. The actual plasmon modes are determined by the zeros of $\epsilon(q,L,w)$. There exist several plasmon modes at given $q$ and $L$, which are denoted by $w_j(q,L)$, $j=1,2,\ldots$. Usually, $w_0(q,L)$ and $w_j(q,L)$ are different.

We can use Eq. (7) to define the oscillator strength of plasmons

$$f_j(q,L)=\left\{w_0^2(q,L)\frac{\partial\,\mathrm{Re}\epsilon(q,L,w)}{\partial w^2}\bigg|_{w=w_j(q,L)}\right\}^{-1}\ , \tag{9}$$

and similarly of the $e$-$h$ excitations

$$f_{e\text{-}h}(q,L)=\frac{2\epsilon_0}{\pi}\int_{\mathrm{Im}\epsilon\neq 0}\frac{w}{w_0^2(q,L)}\mathrm{Im}\left\{\frac{-1}{\epsilon(q,L,w)}\right\}dw\ . \tag{9'}$$

It follows that the total oscillator strength at given $L$ and $q$ is 1 (see Figs. 3 and 5).

In the following calculations we purposely choose $r_1=11$ Å, $m^*=m_e/4$, and $\epsilon_0=2.4$, so that a graphene tubule is closely simulated.[1-4,13] $E_F$ is set at 0.6 eV and hence only the lowest five subbands are occupied. The electron density per unit length is 0.45 Å$^{-1}$. Here we have assumed that the charged carriers are introduced to the graphitic sheet by means of intercalation—as in GIC's. Typical $E_F$ of low-stage GIC's is about 0.5–1.0 eV.[2]

The calculated $L=0$ excitation spectrum is shown in Fig. 2. The shaded region, which is outlined by $E_{\pm}$ of Eq. (6), indicates nonvanishing $e$-$h$ excitations. There are three plasmon branches which all go to zero as $q\to 0$.

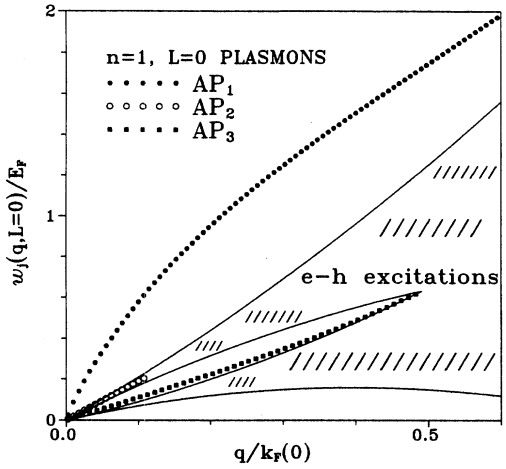


FIG. 2. This is the intrasubband excitation spectrum ($L=0$) for a single tubule ($n=1$) with five populated subbands. The shaded region describes nonvanishing $e$-$h$ excitations. There are three branches of acoustic plasmons (AP's) in the system.

We call them acoustic plasmons (AP's) here. $AP_1$ denotes the most energetic plasmons, $AP_2$ the next energetic plasmons, etc. These AP's may be interpreted as coupled intrasubband plasmons. There are three branches of them since there are three $L=0$ RPA bubbles, respectively, for the $|l|=0$, 1, and 2 subbands [note that $E_{\pm}(q,l,L)=E_{\pm}(q,-l,L)$]. If they were not mutually coupled, the carrier density in $l$ and $-l$ would determine an independent plasmon mode for the subbands, and there are $|l|+1$ of them. The coupling, in general, modifies the plasmon energies but not the number of the collective modes. So, there are $(|l|+1)L=0$ plasmon branches and each one is a collective oscillation of charge carriers from all occupied subbands. The $AP_1$ (solid circles) at small $q$ may be approximated by $w_0(q,L=0)/\sqrt{\epsilon_0}$. One can show that $w_0(q,L=0)\propto q|\ln(qr_1)|^{1/2}$ as $q\to 0$, i.e., $AP_1$ behaves like an ordinary 1D plasmon which corresponds to coherent longitudinal electron density oscillations in the $z$ direction. This $AP_1$ alone almost exhausts the oscillator strength (Fig. 3). The other two branches, $AP_2$ (open circles) and $AP_3$ (solid squares), exist in pockets surrounded by nonvanishing $e$-$h$ excitations. The pocket for undamped $AP_2$ is too small to be shown in the figure. $AP_2$ and $AP_3$ are much weaker than $AP_1$ and would probably be difficult to identify experimentally. The calculated oscillator strength, $f_j(q,L=0)$, is plotted in Fig. 3. The total oscillator strength, with the $e$-$h$ excitations included, equals 1—as it should be from the sum rule, Eq. (7).

Similar plasmon branches of intrasubband excitations in semiconductor QW's have been studied,[14] and the analysis therein is applicable here. The difference is that the exclusion of intersubband excitations is an approximation for the QW's, but is exact for the tubules due to the conservation of $L$. It has been argued[14] that the most energetic intrasubband plasmon is a coherent oscillation of all electrons in the system and hence $f_1(q,L=0)$ dominates. Other plasmon modes (e.g., $AP_2$ and $AP_3$) corre-

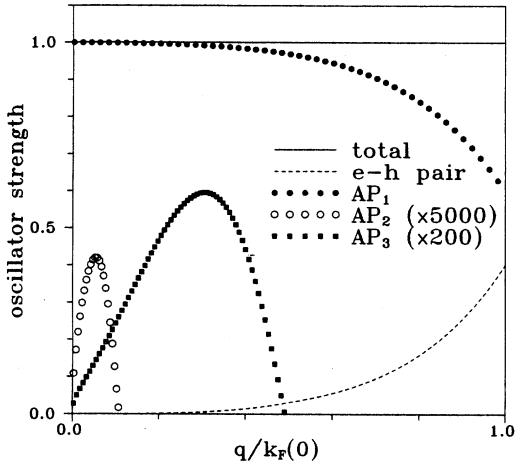


FIG. 3. The oscillator strengths of the three acoustic modes in Fig. 2 are given as functions of $q/k_F(0)$. Also given is the $e$-$h$ contribution (dashed curve). The sum of them (solid curve) equals 1.

spond to incoherent oscillations of different subbands. Their plasmon strengths are therefore weaker; i.e., resonant oscillations coupled to an external field at these plasmon frequencies are weak. The analysis,[14] which is based on an approximation for intrasubband excitations in QW's, can, in fact, be extended to the discussion of intersubband plasmons of the tubular system. This is possible because the $L=0$ (intrasubband) excitation spectra and the $L>0$ (intersubband) spectra are mathematically similar [see Eqs. (5a)–(5c)]. It follows that the excitations of different $L$'s can all be studied independently and evaluated exactly. They share the common features which have already been shown with the $L=0$ case.

The excitation spectrum of the intersubband excitations ($L=1$) is shown in Fig. 4. The shaded regions, as in Fig. 2, are nonvanishing $e$-$h$ excitations. There are five

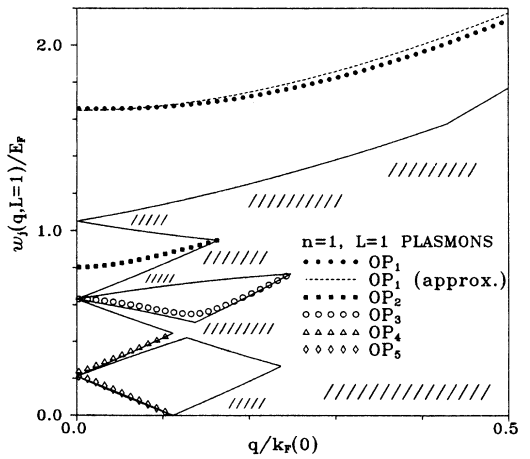


FIG. 4. Same plot as Fig. 2, but for the intersubband ($L=1$) excitations. There are five branches of undamped, optical plasmons (OP's) in the system. The most energetic $OP_1$ branch can be approximated with a quasi-1D plasmon mode (dashed curve) (see the text).

plasmon branches, since each of the five occupied subbands has a different $L=1$ intersubband excitation spectrum. All five plasmon branches approach finite but different values as $q\to 0$. They are called optical plasmons (OP's) here. Similar to the AP's, $OP_1$, $OP_2$, etc., denote the most energetic and the next most energetic optical plasmons, etc. $w_1(q,L=1)$ of $OP_1$ (solid circles) roughly equals $w_0(q,L=1)/\sqrt{\epsilon_0}$ [Eq. (8)] at small $q$. It is interesting to note that $OP_1$ can also be well approximated by $w_0(k,L=0)$ with $k=\sqrt{q^2+1/r_1^2}$ (dashed curve). This fact suggests to us that AP's and OP's are similar 1D oscillations, except that in OP's the minimum momentum transfer is $1/r_1$ instead of zero. Other plasmon branches are confined in the regions between $E_{\pm}(q,l,L=1)$, which correspond to intersubband $e$-$h$ excitation energies and are nonzero at small $q$. Therefore, $L=1$ (or $L\geq 1$) plasmons must be optical plasmons.

The calculated oscillator strength $f_j(q,L=1)$ is given in Fig. 5. The total strength equals 1 at each $q$, as is required by the sum rule, Eq. (7). The intrasubband plasmon analysis[14] can be applied here since the $L=0$ and 1 excitation spectra are similar in structure, as we explained earlier. $OP_1$, which may be considered as a continuation of the quasi-1D plasmon branch, $AP_1$ of $L=0$, represents a coherent oscillation of all carriers in the system; hence, $f_1$ of $OP_1$ dominates. Both $AP_1$ and $OP_1$ carry a longitudinal component (i.e., along the $z$ axis) in their oscillations, but $OP_1$ has an extra transversive component which is a rotational charge oscillation around the tubule. Excitations of the optical plasmons, thus, are expected to accompany quantized magnetic flux inside the tubule. Lower-frequency plasmons (e.g., $OP_2$, $OP_3$,...) correspond to incoherent oscillations of charge carriers from different subbands. They thus have much reduced plasmon strength.

All $L>1$ plasmons can now be readily understood. They are similar in structure to the $L=1$ plasmons but at higher frequencies— because the excitation energies, $E_{\pm}$ of Eq. (6), are higher for $L>1$. There are $2l+1$ optical plasmon branches from the $2l+1$ occupied subbands for

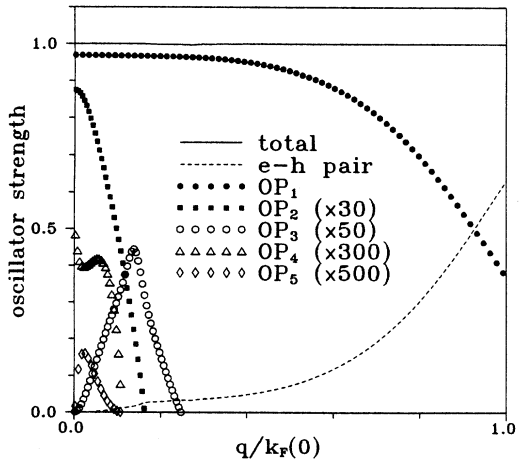


FIG. 5. Same plot as Fig. 3, but for the five OP's of Fig. 4.

each $L$. The most energetic plasmon corresponds to a coherent oscillation of all carriers in the system and has the dominating plasmon strength. This plasmon mode may be interpreted as a quasi-1D plasmon branch at $k=\sqrt{q^2+L^2/r_1^2}$; its dispersion can be well approximated by $w_0(k,L=0)$. Other weaker plasmons are out-of-phase oscillations of different subbands. So, the basic properties of all the plasmon modes are clear in the single-tubule system, and they can be evaluated exactly with the use of Eqs. (4)–(6).

If, instead of the 2D plane waves of Eq. (1), the Bloch states of a graphitic sheet[10] are used, the interaction matrix elements [Eq. (3)] would be modified. However, the azimuthal angle quantization would still be true; hence, the angular momentum conservation would follow. The important features of the tubular plasmons would thus remain valid for graphene tubules. For example, there will be $(l+1)$ $L=0$ AP modes and $(2l+1)$ OP modes for each $L>0$, and excitations of different $L$ can be studied independently. The effect of the inter-$\pi$-band excitations in the graphitic system requires further studies.

## III. EXCITATIONS IN COAXIAL TUBULES

The discussion of excitations is extended here for coaxial tubules. The intertubule separation is assumed large compared with the distance between neighboring atoms on the same tubule. As a result, intertubule hopping is neglected. A similar assumption has been applied, with success, to GIC's (Ref. 10) and is expected to be valid for graphene coaxial tubules.[1] With the exclusion of the hopping, the Coulomb interaction of two electrons on tubules, with the radii $r_i$ and $r_j$, respectively, is given by

$$\begin{aligned} V(q,L;r_i,r_j)&=\langle k+q,l+L;r_i|\langle k'-q,l'-L;r_j| \\ &\quad\times\frac{e^2}{R}|k',l';r_j\rangle|k,l;r_i\rangle \\ &=4\pi e^2 I_L(qr_<)K_L(qr_>)\ , \end{aligned} \tag{10}$$

where $R$ is the distance between the two electrons and $r_<$ ($r_>$) represents the smaller (larger) of $r_i$ and $r_j$. If $r_i=r_j$, the result retrieves to Eq. (3). It is important to notice that the angular momentum (i.e., $L$) is also conserved here. As a result, plasmons of the coaxial tubules have well-defined $L$, too. Also important here is that Eq. (10) is a separable potential in form. As will be discussed below, a modified separable potential [Eq. (14)] could lead to important simplications. The potential of Eq. (10) is shown in Fig. 1. The small-$q$ ($qr_>\ll 1$) behavior is similar to that of a single tubule and exhibits typical 1D character. At $qr_<\gg 1$, the potential may be approximated by $\exp[-q(r_>-r_<)]/q$, which is characteristically the Coulomb interaction in a layered system.[10,15]

Coaxial tubules are more complicated than a single tubule in two essential ways. The first one is related to different zero-energy levels on different tubules. Charge carriers, by assumption, are introduced onto the tubules through intercalation, as in GIC's.[2,10] Consider a neutral tubular system with intercalants (as donors or acceptors). At thermal equilibrium, there is but one chemical potential (i.e., $E_F$) for the system, but charges on different tubules experience different Coulomb potentials, $\Delta U(r_i)$, where $\Delta U(r_1)=0$. Here and thereafter, we use $r_i$ to indicate the $i$th tubule and let $r_1<r_2<r_3$, etc. $r_1$ thus denotes the innermost tubule. $\Delta U(r_i)$ and $E_F$ need to be self-consistently determined in accordance with the doping concentration and the distribution of the intercalants. Once $\Delta U(r_i)$ have been determined, their only effect is to be included in the electron energy $E(k,l;r_i)=\Delta U(r_i)+(k^2+l^2/r_i^2)/2m^*$ for the rest of the calculations.

The formalism to be developed below is applicable to any $n$-tubule coaxial system. But only the following $n=2$ model system is calculated for the purpose of illustration. It has $r_1=11$ Å and $r_2=14.4$ Å (Ref. 1) and the intercalants are assumed to distribute uniformally along the common axis of the cylinders. $\epsilon_0=2.4$, $m^*=m_e/4$, and $E_F=0.6$ eV, as in Sec. II. These numbers are reasonable for graphene tubules and correspond to a doping concentration of 0.91 Å$^{-1}$. There are five subbands in each of the two tubules and $\Delta U(r_2)=0.12$ eV.

The second complication for the coaxial tubules results from the mutual coupling among the tubules; i.e., charge fluctuations on one tubule influence the charges on other tubules. Consider an external potential on the $i$th tubule, $v_i^{\rm ex}(q,L)$, which induces $v_j^{\rm in}(q,L)$ on the $j$th tubule. The total effective potential is $v_i^{\rm eff}(q,L)=v_i^{\rm ex}(q,L)+v_i^{\rm in}(q,L)$. Within the linear-response theory, $v_i^{\rm in}$ is proportional to $v_i^{\rm eff}$. There thus exists a linear relation

$$v_i^{\rm eff}(q,L,w)=v_i^{\rm ex}(q,L,w)+\sum_j \epsilon_{ij}v_j^{\rm eff}(q,L,w)\ . \tag{11}$$

The dielectric function $\epsilon_{ij}$ can be obtained from the self-consistent-field method:[11]

$$\epsilon_{ij}(q,L,w)=\epsilon_0\delta_{ij}-V(q,L;r_i,r_j)\chi_j(q,L,w)\ . \tag{12}$$

$\chi_i$ is the response function of the $i$th tubule and is expressible by Eqs. (5) and (6); i.e., $\chi$ of a single tubule. The constant energy shift, $\Delta U(r_i)$, only affects $k_F(l,r_i)$ of Eq. (6). Linear screening relations similar to Eqs. (11) and (12) had been derived for GIC's.[10]

Equation (11) is an $n\times n$ matrix equation for an $n$-tubule system. The plasmons of the system are given by $\det[\epsilon_{ij}(q,L,w)]=0$. When the coupling among tubules is turned off [i.e., setting $V(q,L;r_i,r_j)=0$ if $r_i\neq r_j$], $\epsilon_{ij}$ becomes diagonal and plasmons are just the single-tubule plasmons given by Eq. (4). This is reasonable since tubules in this case are independent of each other. Complication from the coupling is, mathematically, in the nonlinear interaction terms. Take the $n=2$ case, for example. Plasmons are determined by

$$\begin{aligned} &\epsilon_0-V(r_1)\chi_1-V(r_2)\chi_2 \\ &\quad+\frac{1}{\epsilon_0}[V(r_1)V(r_2)-V(r_1,r_2)V(r_2,r_1)]\chi_1\chi_2=0\ , \end{aligned} \tag{13}$$

where nonessential parameters have been suppressed. The $L=0$ and $L=1$ plasmons, respectively, are shown in Figs. 6 and 7. Only the two most energetic branches

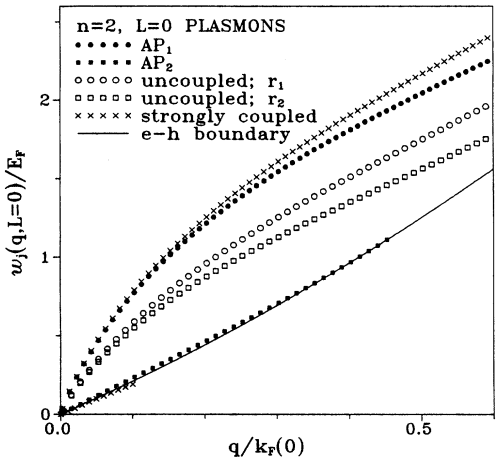


FIG. 6. The intrasubband ($L=0$) excitation spectrum of two coaxial tubules ($n=2$). Only the two most energetic plasmon branches are given. If the intertubule interaction is switched off, the plasmons are just those of individual tubules (open circles and squares). The plasmons of coupled tubules can be well approximated in the strong-coupling picture (crosses) described by Eq. (16). The solid curve depicts the boundary of the $e$-$h$ excitations, below which plasmons may be Landau-damped.

(solid circles and squares) in each case are given; other plasmon modes are weak in strength and rapidly diminish due to the electron-hole-pair excitations. Also plotted in the figures are plasmons from uncoupled tubules (open circles and squares). Modification of the plasmon modes due to the coupling is clearly very important.

The plasmons of the coupled tubules can be approximately understood in terms of Eq. (13) but with its nonlinear terms neglected. Plasmons determined this way (crosses in Figs. 6 and 7), in fact, agree closely with the exact results. This is especially true for small $q$. Linearized Eq. (13) can be expressed as $\epsilon_0-\sum_{i=1}^{2}\sum_{l}^{\text{occ}}V(r_i)\chi_i^l=0$; which is very similar to Eqs.

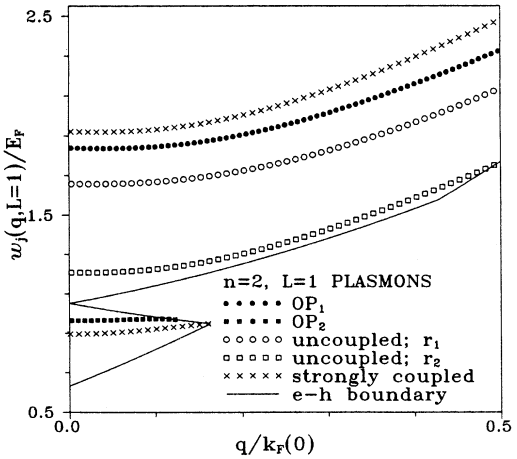


FIG. 7. Same plot as Fig. 6, but for the intersubband ($L=1$) OP's. The strong coupling remains a reasonable approximation, but not as good as in the $L=0$ case (see the text).

(4) and (5) of a single tubule. $\chi_i^l$ is understood to be the response function of the subband $l$ in the $i$th tubule. So an $n=2$ system is not more complex than a single tubule in this picture. The only difference is that the two systems have different numbers of occupied subbands: five subbands in Sec. II but ten now (with five from each tubule). Similar arguments that have been employed in Sec. II can now be readily applied here. One can easily figure out that there are six $L=0$ acoustic plasmon branches and ten optical plasmon branches for each $L>1$. At a given $L$, the most energetic plasmon mode, which corresponds to coherent oscillations of all electrons, by and large exhausts the plasmon strength; other modes are much weaker and are associated with incoherent oscillations of electrons from different subbands. So, as long as the nonlinear potential terms can be neglected, multitubule plasmons can be readily understood based on the analysis given in Sec. II.

Several factors help explain why neglecting high-order interactions makes good approximations here. The high-order terms actually come in powers of $(V/\epsilon_0)$. Thus the approximation improves with increasing $\epsilon_0$. In GIC's, the interband transitions, which have been neglected here, enhance $\epsilon_0$ from 2.4 to about 6.0.[10] Our calculation indicates that the error due to the linearization of Eq. (13) could be reduced by $\sim 50\%$ if $\epsilon_0$ is 6.0 instead of 2.4. Thus the approximation is expected to work well for graphene tubules.

Also, a large cancellation between the nonlinear terms in Eq. (13) is observed. The cancellation becomes exact if $r_2 \to r_1$, which corresponds to an increase of the intertubule coupling. This $n=2$ result can be generalized to other $n$'s. In the Appendix, w show that if the potential is separable, i.e.,

$$W(r_i,r_j)=Q(r_i)Q'(r_j)\ , \tag{14}$$

and has the property

$$Q(r_i)Q'(r_j)=Q(r_j)Q'(r_i)\ , \tag{14'}$$

the plasmons would be exactly given by the linearized relation $[W(r_i)=W(r_i,r_i)]$

$$\epsilon_0-\sum_{i=1}^{n}\left\{W(q,L;r_i)\left[\sum_{l}^{\text{occ}}\chi_i^l(q,K,w)\right]\right\}=0\ . \tag{15}$$

This result is good for any $n$. The intertubule interaction, Eq. (10), does not fulfill Eq. (14'). We may, however, define a modified potential:

$$V'(r_i,r_j)=[V(r_i)V(r_j)]^{1/2}\ . \tag{16}$$

This potential $V'$ clearly satisfies Eqs. (14) and (14'), and equals $V(r_i)$ if $r_i=r_j$. Take the $n=2$ case, for example. The nonlinear interaction terms of Eq. (13) obviously cancel out if $V$ is replaced by $V'$. Plasmons determined from Eq. (15) with $W=V'$, thus, are exact for the interaction $V'$ and approximate for $V$. $V'$ is always greater than $V$, as can be checked for the $n=2$ case using Fig. 1.

We may thus interpret these plasmons of $V'$ as the strong-coupling approximation. Plasmons in the weak-coupling limit, where $V(r_i,r_j)=0$ if $r_i \neq r_j$, have been found to be just those of individual tubules. It seems reasonable to expect plasmons of a coaxial-tubule system to lie between these two coupling limits. This is clear in the case with our $n=2$ results.

We noted earlier that the intertubule interaction at small $q$ behaves like a single-tubule interaction and at large $q$ like a typical interlayer interaction, which carries a factor $\exp[-q(r_> - r_<)]$. As a result, the plasmons of coaxial tubules are well described by the strong-coupling approximation at small $q \ll (r_> - r_<)^{-1}$ but become more and more weakly coupled as $q$ increases. For intersubband plasmons (i.e., $L \neq 0$), the effective momentum transfer is $\sim k = \sqrt{q^2 + L^2/r^2}$—as was argued in Sec. II. Therefore the strong coupling becomes a poorer approximation as $L$ increases. At very large $L$, all tubules become independent of each other and their plasmons are those of individual tubules, i.e., in the weak-coupling limit. So, there is a gradual crossover from strong coupling to weak coupling as $q$ increase, and also as $L$ increases. This trend is seen clearly in Figs. 6 and 7. At both of the coupling limits, the plasmon structures are simple and easy to understand based on the analysis presented in this work.

The background dielectric constant of graphene tubules should be enhanced due to the inter-$\pi$-band excitations, which have been neglected here. A large dielectric constant would make the nonlinear interaction unimportant—which effectively validates the strong-coupling approach [see Eq. (13)]. Our calculation indicates that both the $L=0$ and 1 plasmons of coaxial graphene tubules, which have an estimated dielectric constant of about 6.0, can be fairly well described within the strong-coupling approximation.

## IV. CONCLUDING REMARKS

In this work, we have studied the elementary excitations of an electron gas confined to cylindrical tubules. Exact results within the RPA have been evaluated for a single tubule ($n=1$) and also for an $n=2$ coaxial system. The results are then generalized for $n$ coaxial tubules. In the $n>1$ cases, the interaction between electrons from different tubules has been included. The calculations suggest that the plasmons of small $q$ and small $L$ can be well described in the strong-coupling picture, which is summarized by Eq. (15).

The cylindrical symmetry of the tubular system greatly simplifies the problem. The symmetry ensures the conservation of the angular momentum, $L$. As a result, plasmons of different $L$'s are decoupled from each other. In contrast to other quasi-1D systems (e.g., semiconductor wires) where plasmon modes are mostly coupled together, the coaxial tubule system allows us to study all its quasi-1D plasmons in a systematic way.

Besides the very interesting quasi-1D behavior discussed in this work, tubules also resemble the fascinating ring system made of metals.[16–18] It has been established that[16–18] the persistent current in small rings is a periodic function of the enclosed magnetic flux. It should be noticed that the $L \neq 0$ plasmons in the tubular system correspond to quantized, rotational charge oscillations. This quantized current in a tubule clearly resembles the persistent current in a ring. One can thus expect the magnetoplasmons of a tubule to exhibit a similar periodic behavior if the magnetic flux is varied. This problem is under current investigation.

## ACKNOWLEDGMENTS

K. S. thanks G. D. Mahan and others at Oak Ridge National Laboratory for their hospitalities. This work was supported in part by the National Science Council of Taiwan, the Republic of China under Grant Nos. NSC 81-0208-M-007-09 and NSC 82-0208-M-007-008.

## APPENDIX

In this appendix we show the validity of the dielectric function given by Eq. (15) for the potential expressed by Eqs. (14) and (14′). This can be seen most clearly with diagrams. The screening of the potential $W(r_i,r_j)$, within the RPA, contains a series of "bubbles," as shown by Fig. 8(a). A bubble denoted by $r_i$ represents an electron-hole pair in the $i$th tubule. The electron and the hole must be on the same tubule since there is no intertubule hopping. Figure 8(b) is a typical third-order diagram which contains three bubbles. For the reason that the interaction potential is separable [Eq. (14)] and is symmetric under the exchange of $r_i$ and $r_j$ [Eq. (14′)], the two vertices of a bubble at $r_i$ can always be associated with one $Q(r_i)$ and one $Q'(r_i)$, as indicated in Fig. 8(b). The contribution of a bubble at $r_i$ is therefore always given by $W(r_i)\chi_i/\epsilon_0$ $[W(r_i)=W(r_i,r_i)]$. Figure 8(b), for example, represents

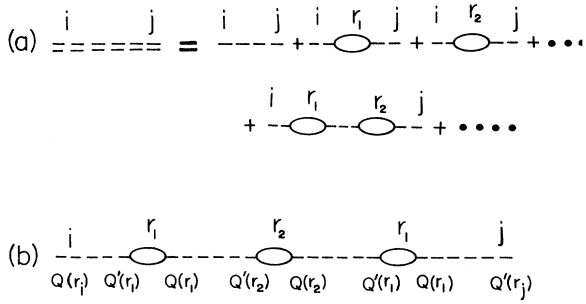


FIG. 8. (a) Expansion diagrams of screened Coulomb interaction (double-dashed curve). Single-dashed curves represent unscreened interaction. Bubbles denoted by $r_i$ represents an $e$-$h$ pair in the $i$th tubule. (b) A typical third-order diagram is shown, where the vertices have been indicated in accordance with the potential given by Eqs. (14) and (14′).

$W(r_i,r_j)[W(r_1)\chi_1/\epsilon_0]^2[W(r_2)\chi_2/\epsilon_0]$. For an $n$-tubule system, a diagram with $m_1$ $r_1$ bubbles, $m_2$ $r_2$ bubbles, etc., is hence given by $W(r_i,r_j)\prod_k^n[W(r_k)\chi_k/\epsilon_0]^{m_k}$, and these $M=\sum_k^n m_k$ bubbles can appear in $M!/m_1!/m_2!\ldots$ different combinations. These $M$th-order diagrams can be summarized by $W(r_i,r_j)[\sum_k^n W(r_k)\chi_k/\epsilon_0]^M$. The screened potential is therefore

$$W(r_i,r_j)/\epsilon(q,L,w) = W(r_i,r_j)\left\{1+\sum_{M=1}^{\infty}\left[\sum_k^n W(r_k)\chi_k/\epsilon_0\right]^M\right\}, \quad \text{(A1)}$$

which is just the definition of the dielectric function of Eq. (15).


[1]S. Iijima, Nature **354**, 56 (1991).

[2]M. S. Dresselhauss, *Intercalation in Layered Materials* (Plenum, New York, 1987).

[3]Y. Chai, T. Guo, C. M. Jin, R. E. Haufler, L. P. Felipe Chibante, J. Fure, L. H. Wang, J. M. Alford, and R. E. Smalley, J. Phys. Chem. **95**, 7564 (1991).

[4]M. F. Lin and K. W. -K. Shung, Phys. Rev. B **46**, 12 656 (1992).

[5]M. S. Dresselhaus, G. Dresselhaus, and R. Saito, Phys. Rev. B **45**, 6234 (1992).

[6]Q. P. Li and S. D. Sarmas, Phys. Rev. B **40**, 5860 (1989); **43**, 11 768 (1991); Q. P. Li, S. D. Sarmas, and R. Joynt, *ibid.* **45**, 13 713 (1992).

[7]T. Demel, D. Heitmann, P. Grambow, and K. Ploog, Phys. Rev. B **38**, 12 732 (1988).

[8]S. D. Sarmas and W. Y. Lai, Phys. Rev. B **32**, 1401 (1985).

[9]G. Y. Hu and R. F. O'Connel, Phys. Rev. B **42**, 1290 (1990).

[10]K. W.-K. Shung, Phys. Rev. B **34**, 979 (1986); **34**, 1264 (1986).

[11]H. Ehrenreich and M. H. Cohen, Phys. Rev. **115**, 786 (1959).

[12]D. Pines and P. Nozières, *The Theory of Quantum Liquids* (Benjamin, New York, 1966).

[13]E. A. Taft and H. R. Philipp, Phys. Rev. **138**, A197 (1965).

[14]B. S. Mendoza and Y. C. Lee, Phys. Rev. B **40**, 12 063 (1989).

[15]T. Ando, A. B. Flowler, and F. Stern, Rev. Mod. Phys. **54**, 437 (1982).

[16]H. F. Cheung, Y. Gefen, E. K. Riedel, and W. H. Shih, Phys. Rev. B **37**, 6050 (1988).

[17]U. Eckern and A. Schmid, Europhys. Lett. **18**, 457 (1992).

[18]B. Altshuler, Y. Gefen, and Y. Imry, Phys. Rev. Lett. **66**, 88 (1992).